

The Evolution of the Ozone “Collar” in the Antarctic Lower Stratosphere during Early August 1994

ANNARITA MARIOTTI

ENEA, Ocean–Atmosphere Dynamics Group, Rome, Italy

CARLOS R. MECHOSO

Department of Atmospheric Sciences, University of California, Los Angeles, Los Angeles, California

BERNARD LEGRAS AND VINCENT DANIEL

Laboratoire de Météorologie Dynamique, CNRS, Paris, France

(Manuscript received 27 July 1998, in final form 15 March 1999)

ABSTRACT

The ozone evolution in the lower stratosphere of the Southern Hemisphere during the period 5–10 August 1994 is analyzed. The analysis focuses on the ozone “collar” (the band of maximum values in ozone mixing ratio around the Antarctic ozone “hole” at these altitudes) and the development of “collar filaments.” Ozone mixing ratios provided by the Microwave Limb Sounder (MLS) on board the *Upper Atmosphere Research Satellite* and by an ER-2 aircraft participating in the Airborne Southern Hemisphere Ozone Experiment/Measurements for Assessing the Effects of Stratospheric Aircraft campaign are compared with values at corresponding locations in high-resolution isentropic maps obtained by using the numerical scheme of “contour advection with surgery” (CAS).

The CAS reconstructed ozone maps provide a view of the way in which air masses are exported from the outskirts of the collar to form the “tongues” of higher mixing ratios observed at lower latitudes on MLS synoptic maps. There is an overall consistency between the datasets insofar as the collar location is concerned. This location seems to be primarily defined by the local properties of the flow. Nevertheless the CAS reconstructed collar tends to become weaker than that depicted by MLS data. By means of radiative calculation estimates, it is argued that diabatic descent may be responsible for maintaining the ozone concentration approximately constant in the collar while filaments isentropically disperse collarlike mixing ratios from this region toward lower latitudes.

1. Introduction

In this paper we examine the evolution of ozone mixing ratios in the lower southern stratosphere during a five-day period of the mid- to late winter. Specifically, we select the 510-K and 470-K potential temperature surfaces and the period 5–10 August 1994. At those levels and times, the ozone “hole” is an outstanding feature of the ozone distribution. There is broad consensus on the processes that lead to the ozone hole formation. During the mid- to late southern winter the polar night vortex isentropically isolates the polar regions from lower latitudes (McIntyre 1989; Hartmann et al. 1989; Schoeberl et al. 1992; Bowman 1993; Chen 1994). Inside the vortex descent rates are weak and

ozone mixing ratios are mainly determined by chemical effects (Rosenfield et al. 1994; Manney et al. 1995a,c). A chemically perturbed region (CPR) appears as temperatures become low enough for polar stratospheric cloud formation, and sunlight activates catalytic reaction cycles responsible for ozone depletion (Schoeberl and Hartmann 1991).

Also in the lower southern stratosphere during the late southern winter, data from the Microwave Limb Sounder (MLS) on board the *Upper Atmosphere Research Satellite* (UARS) typically show a “collar” of higher ozone mixing ratio around the ozone hole (Waters et al. 1993; Manney et al. 1995b). At approximately the same location, data provided by the Cryogenic Limb Array Etalon Spectrometer (also on board UARS) reveal the existence of a collar of higher ClONO₂ mixing ratios (Roche et al. 1994). The enhanced ClONO₂ concentrations are the result of ClO deactivation by NO₂ (Chipperfield et al. 1997) and indirectly an indicator that in this region ClO is not active in destroying ozone.

Corresponding author address: Carlos R. Mechoso, Department of Atmospheric Sciences, University of California, Los Angeles, Los Angeles, CA 90095-1565.
E-mail: mechoso@atmos.ucla.edu

Dynamical and chemical effects may cooperate to produce the ozone collar. Studies of the dispersion properties of the flow in polar regions have demonstrated that the vortex core is surrounded by a highly energetic strain-dominated circulation (Trunday et al. 1995; Paparella et al. 1997). Quasi-isentropic large-scale motion associated with planetary wave propagation and breaking is responsible for the formation of “vortex filaments,” which can carry air from the outskirts of the vortex toward lower latitudes (Jukes and McIntyre 1987; Polvani and Plumb 1992; Bowman and Mangus 1993; Chen et al. 1994; Bowman 1993; Waugh et al. 1994; Schoeberl and Newman 1995; Manney et al. 1995c; Newman et al. 1996; Mariotti et al. 1997; Orsolini et al. 1997). The vortex filaments may also contribute to enhanced chemical processes in the ozone collar by stretching around the vortex core and favoring mixing between air masses from polar and midlatitudes in a way similar to that suggested by Chipperfield et al. (1997) for the ClONO₂ collar.

In this study we aim to better understand the evolution of the ozone collar by contrasting MLS ozone values to their counterparts in reconstructed isentropic maps obtained with the high-resolution numerical scheme of “contour advection with surgery” (CAS) (Waugh and Plumb 1994; Norton 1994). The input to the CAS algorithm consists of 1) the global-synoptic ozone fields derived from MLS data (version 3) calculated using the method of Elson and Froidevaux (1993) and 2) the horizontal wind distributions provided by analyses compiled at the European Centre for Medium-Range Weather Forecasts (ECMWF).

The CAS calculations assume that fluid parcels conserve 1) potential temperature and 2) ozone mixing ratio. Satellite measurements and temporal sequences of winds from meteorological analyses have been used by several authors to attempt a “reconstruction” of unresolved features on global satellite maps (Pierce et al. 1994; Sutton et al. 1994; Morris et al. 1995). Manney et al. (1995a,c) performed three-dimensional Lagrangian calculations to estimate the relative impact of diabatic and chemical effects on the ozone distribution. These authors find that descent over Antarctica in late winter is mostly concentrated on the outskirts of the vortex and that descent rates are generally weak (0.4 K day⁻¹) below 520 K. They also find that vortex averaged mixing ratios are mainly determined by chemical effects.

On short timescales and outside the CPR, however, transport processes, both isentropic and diabatic, may still play an important role in determining the ozone distribution. To address this issue we follow a two-pronged approach. First, we compare the results of our CAS isentropic calculations with MLS data along the satellite’s orbits. We also perform a similar comparison with data obtained by an ER-2 aircraft participating in the Airborne Southern Hemisphere Ozone Experiment/Measurements for Assessing the Effects of Stratospheric

Aircraft (ASHOE/MAESA) campaign. Second, we calculate diabatic descent rates using the radiative code of the ECMWF model (Mocrette 1991) and estimate their impact on the ozone collar concentrations.

The paper starts in section 2 by presenting a description of the data. Section 3 investigates the ozone evolution at 510 K during the period 5–10 August 1994. In this context, we examine MLS synoptic fields and CAS reconstructed maps and discuss the reconstructed features through direct comparisons with MLS orbit data (Level 3AT, at 65.536-s centers resolution). Here we also compare MLS synoptic data at 470 K, CAS-reconstructed maps, and ER-2 data. Section 3 also presents the results from our diabatic descent rate calculations. Section 4 includes a discussion of results and presents our conclusions.

2. Description of data

a. Satellite and aircraft data

The MLS instrument on board the *UARS* (Reber 1990) has been providing measurements of ozone and other atmospheric constituents throughout the stratosphere since late September 1991. The satellite covers a geographical domain extending from 80° latitude in one hemisphere to 34° in the other at a rate of 15 orbits per day during a 36-day-long period. At the end of the period the satellite switches over by a 180° rotation to alternatively cover both hemispheres. Our analysis starts on 5 August 1994, when the *UARS* turned to observe the Southern Hemisphere. The ozone data were obtained by the MLS 205-GHz radiometer described by Barath et al. (1993). The measurements were performed according to the technique presented by Waters (1993) and were retrieved and validated as described in Froidevaux et al. (1996). The MLS instrument scans the atmospheric limb at 90° to the satellite velocity vector, providing an atmospheric profile once every 65.5 s approximately every 400 km along the satellite track. Each profile is an “average” over a similar distance along the line of sight. We use MLS data version 3. In the lower stratosphere Froidevaux et al. (1996) estimate that this data has an (rms) accuracy of the order of 0.3 parts per million volume (ppmv) and an effective vertical resolution of approximately 4 km, which is about 80 K.

The ozone data from the ER-2 aircraft participating in the ASHOE/MAESA campaign (Tuck et al. 1997) was obtained by the ER-2 UV absorption photometer (Proffitt et al. 1989). We use information collected along sections of the flights performed at about 470 K (between 460 K and 490 K) on 8 and 10 August 1994. All measurements in this altitude range were linearly interpolated to the 470-K surface using a vertical gradient also estimated from the ER-2 data. The aircraft took off from Christchurch, New Zealand (43°S, 172.5°E), and also sampled other atmospheric constituents as well as temperature along the flight track with a horizontal sam-

pling of approximately 1 km (1-Hz measuring frequency).

b. Data for the CAS calculations

MLS synoptic ozone distributions were derived from the MLS data on *UARS* pressure levels according to Elson and Froidevaux (1993) at 1200 UTC on each day during the selected period. Those distributions have a grid size of 4° lat \times 5° long on pressure levels. The data processing for this study consisted of three steps. First, the ozone distributions were regridded to the grid of the ECMWF wind analysis using a vertical interpolation from *UARS* pressure levels to ECMWF pressure levels and a horizontal interpolation with a bilinear scheme from the 4° lat \times 5° long grid to a Gaussian grid with 128×32 points per hemisphere. Second, ozone and wind components were vertically interpolated as in Brunet et al. (1995) to obtain fields at selected isentropic levels. Third, the resulting fields were expanded in terms of spherical harmonics and mapped onto a Gaussian grid with 256×96 points per hemisphere.

A 30-min time step is used for the advection calculations and a cubic spline scheme to interpolate in time the wind data, which is originally available at 6-h time intervals. Southern Hemisphere wind analyses suffer from a sparseness of direct measurements. Since we perform isentropic calculations, we apply a low-pass filter to the divergent component of the isentropic wind, which is very noisy on synoptic timescales. Contours for the initial ozone distribution are obtained by calculating isolines at discrete mixing ratio values. The discretization interval is 0.2 ppmv, which is slightly smaller than the estimated uncertainty of MLS data. The spatial resolution of the CAS calculations depends on the density of the nodes used to define the contours, which is controlled by the parameter μ , and on the critical distance between the contours δ , which define the threshold for surgery to take place. Here we select the CAS parameters to allow for a resolution of about 20 km. Further details on the CAS scheme as it is used in this study are given in the appendix.

c. Data for diabatic descent rates calculations

The diabatic descent rates are calculated from the thermodynamic equation in which diabatic heating rates are obtained using the radiative code of the ECMWF model (Morcrette 1991). This algorithm is based on narrowband models in which Voigt line shape is used for the upper levels. The radiative descent is calculated for clear sky using temperatures retrieved from the ECMWF analysis. The CO_2 profile is prescribed from the climatology, while the ozone profile is taken from MLS data interpolated to the model levels. The resulting descent is then combined with the vertical derivative of

ozone mixing ratio calculated on MLS levels to provide the vertical ozone transport $(D\theta/Dt)(\partial[\text{O}_3]/\partial\theta)$.

3. Results

a. CAS reconstructed ozone fields

Figure 1 shows MLS orbit ozone and ECMWF potential vorticity (PV) as a function of latitude at 510 K along the *UARS* orbit at about 1200 UTC on 8 August 1994. As MLS samples the ozone distribution when the satellite is approaching the pole or moving away from it, mixing ratios have larger values in a latitude band of approximately 20° to 30° width centered at about 55°S . We will refer to this band as the “ozone collar.” There are other narrow bands with minimum mixing ratios along both the poleward and equatorward flanks of the collar (inner and outer edge, respectively). Figure 1 shows enhanced PV gradients near the ozone maxima. According to Jukes and McIntyre (1987) and McIntyre (1989), these high gradients mark the “dynamical edge” of the vortex. Synoptic plots of ECMWF wind also at 510 K (not shown) indicate that the stratospheric jet core is approximately within the collar region.

The MLS synoptic ozone fields at 510 K on each day from 5 to 10 August 1994 are shown in Fig. 2. The region with mixing ratios greater than ~ 3.3 ppmv around the Pole corresponds to the ozone collar. This feature evolves from a pattern with a strong zonal wave-number-2 component on 5 August toward a nearly zonal symmetric configuration by 10 August. Figure 3 shows the CAS reconstructed ozone maps in a calculation from initial conditions on 5 August 1994, for the same period covered in Fig. 2. On the larger scales, the evolution of the ozone collar in the maps of Figs. 2 and 3 is generally similar. The CAS reconstructed maps reveal a fine structure inside the collar with a tendency to progressively thin out during the period. The map for 8 August in Fig. 2d shows a trough in the lower left quadrant, as the collar is locally displaced toward the equator. The maps for 9 and 10 August in Figs. 2e and 2f show an eastward translation and progressive weakening of the trough. The CAS reconstructed maps capture this feature even more sharply showing a breaking of the trough on 10 August.

Outside the collar, the MLS synoptic fields of Fig. 2 show pools of lower mixing ratio (~ 2.7 ppmv). The intermediate regions with higher mixing ratios (~ 3.3 ppmv) appear as “tongues” of air from the vortex body. One large pool of lower mixing ratios is in the lower right quadrant of Fig. 2a, straddling the collar and a tongue of higher mixing ratios on the equatorward side. This pool moves eastward to appear in the lower left quadrant of Fig. 2d, has a considerably smaller size in Fig. 2e, and has practically disappeared in Fig. 2f. On 10 August, another tongue of air with higher mixing ratios stretches across the upper left quadrant of Fig. 2f.

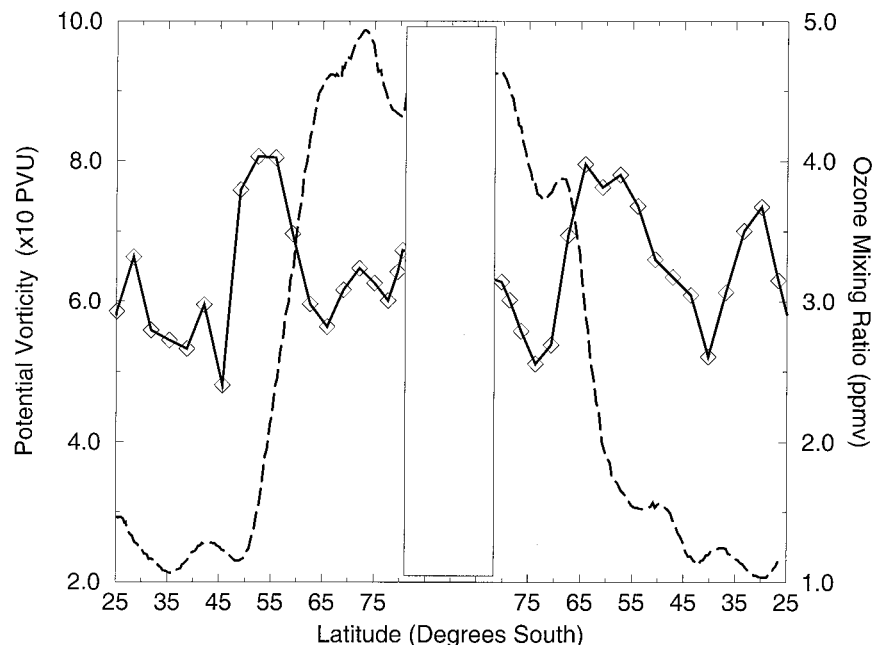


FIG. 1. MLS ozone (ppmv) at 510 K (solid line with diamonds) and ECMWF PV (absolute values in PVU, $1 \text{ PVU} = 10^{-6} \text{ km}^2 \text{ s}^{-1} \text{ kg}^{-1}$, dashed line), as a function of latitude along the UARS orbit at 1200 UTC on 8 Aug 1994. The shaded area represents the region where MLS data are unavailable.

The sequence of snapshots in Fig. 3 offers a reconstruction of how the air masses from the vortex body may evolve to form planetary-scale features in the ozone distribution. On 8 August the CAS reconstructed maps show two major sets of filaments spanning the upper left and the lower left quadrant of Fig. 3d, both of which are separated from the collar by regions of low mixing ratios. Figures 3e and 3f show how these filaments wrap around the vortex and form, by 10 August, numerous secondary structures. However, unlike in the MLS synoptic field of Fig. 2f, a region of low mixing ratio persists in the lower left quadrant of Fig. 3f between the equatorward flank of the collar and the filament.

The CAS reconstructed maps of Fig. 3 also show a population of finer filaments with horizontal scales smaller than those that can be resolved by the MLS synoptic fields. The collar itself appears as an ensemble of thin filaments wrapping around the vortex core. At times, these filaments stretch out from the collar and export air with high mixing ratios toward lower latitudes. These features do not have a clear counterpart in the MLS synoptic fields of Fig. 2, in which higher mixing ratios are primarily confined to the collar. The CAS reconstructed filaments progressively cascade to finer scales and are eventually eliminated by the “surgery” component of CAS (see section 4 and the appendix). On 10 August, the lower right quadrant of the map in Fig. 3f shows filaments in an advanced cascading stage. The corresponding region in Fig. 2f instead presents homogeneous mixing ratios, whose values are roughly

equal to the area average of those in the CAS reconstructed maps in Fig. 3f for the same region.

As a measure of the agreement between the MLS orbit and the corresponding CAS reconstructed values we calculate the linear correlation coefficient between the two datasets, in which the latter was spatially averaged to match the resolution of the former. Figure 4a shows this correlation coefficient as a function of time. The initial correlation coefficient is 0.9 since the CAS calculation is initialized with the MLS synoptic ozone field, which results from an interpolation of MLS orbit data. The correlation rapidly drops to 0.75 by day 1 and then more gradually to 0.7 by day 5. For comparison, we also plot in Fig. 4a the persistence correlation coefficient between MLS orbit data and the initial MLS synoptic ozone field. The two curves in Fig. 4a are very close to each other at the beginning of the calculation but differ by about 0.1 toward the end. Figure 4b shows the correlation coefficient along each orbit between MLS orbit data and nonspatially averaged CAS reconstructed values. The curve in Fig. 4b shows large fluctuations starting early on in time, with values as low as about 0.4 after day 1 and as high as about 0.8 for some orbits around day 3.

Further insight into the nature of the differences between MLS orbit ozone data and CAS resolution-degraded data can be gained from Fig. 5a and 5b, which show the mean and the variance of the MLS orbit and CAS reconstructed data, respectively, by latitude bins of 0.5° for the period 5–10 August. Most relevant in Fig. 5a is the difference between the two latitude means

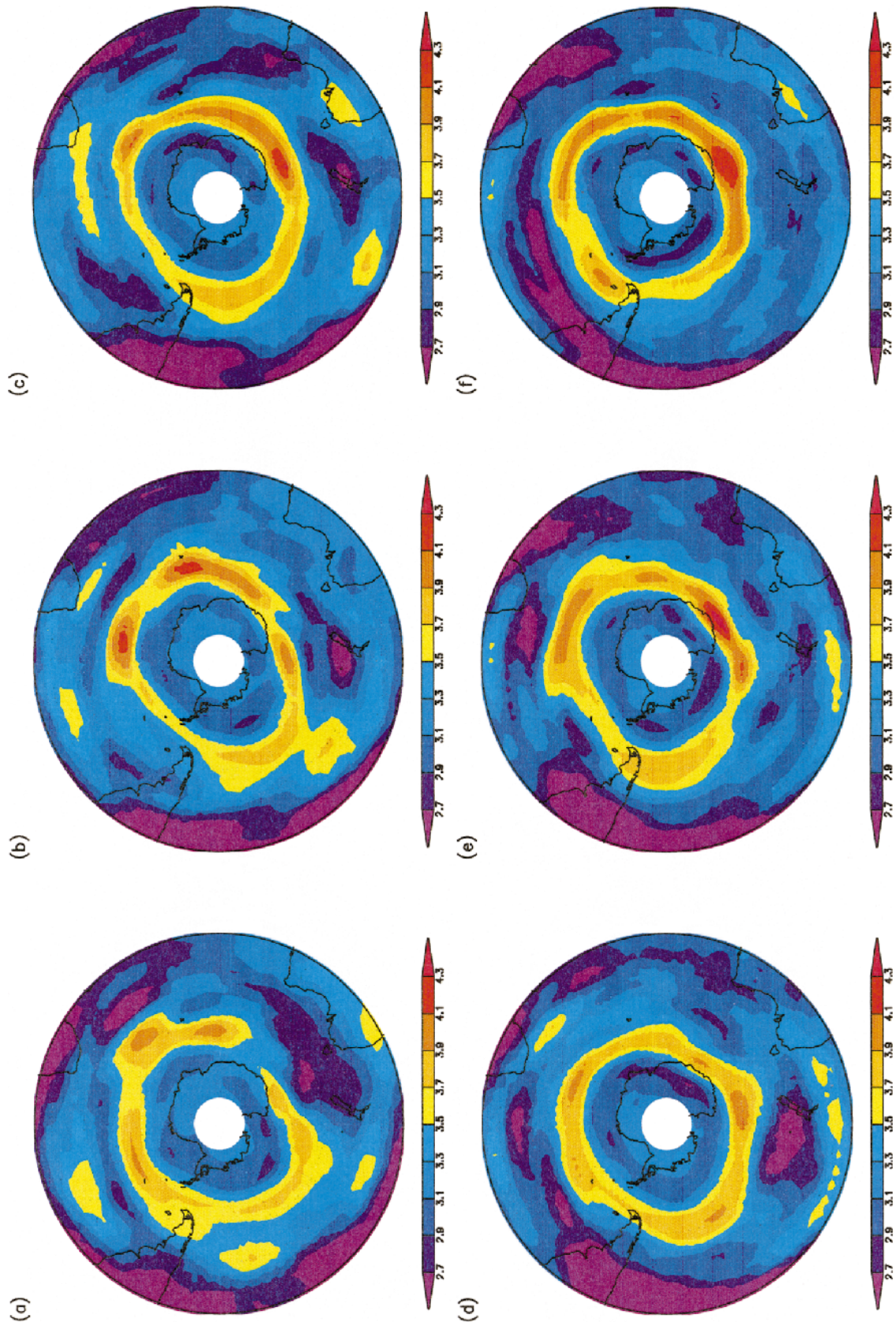


FIG. 2. MLS synoptic ozone fields at 510 K and 1200 UTC on (a) 5 Aug, (b) 6 Aug, (c) 7 Aug, (d) 8 Aug, (e) 9 Aug, and (f) 10 Aug 1994. The projection is stereographic about the South Pole and extends equatorward to latitude 25°S. The white circle centered over the Pole marks the area where no data was available. (Scale in ppmv.)

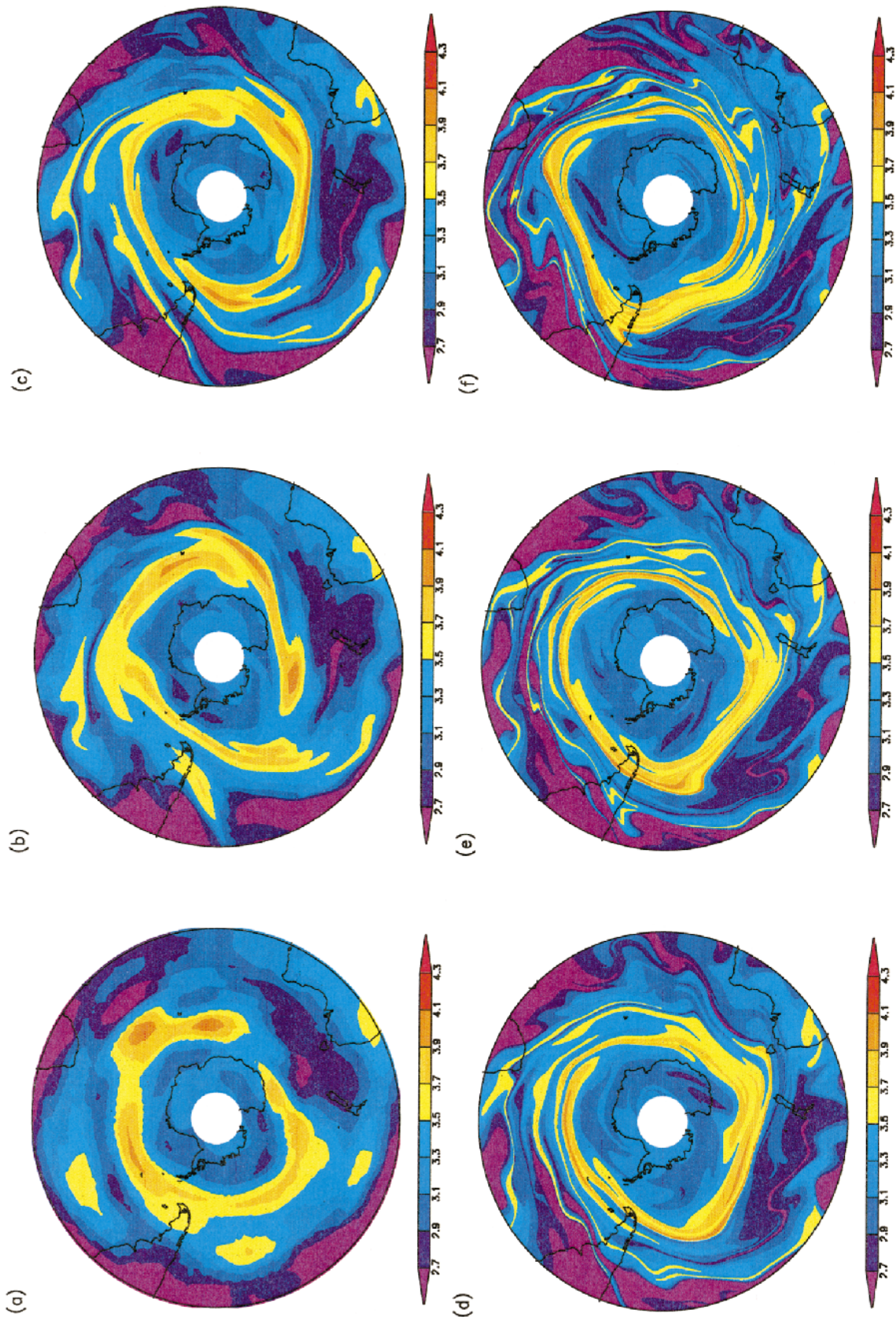


FIG. 3. As in Fig. 2, except for CAS reconstructed ozone maps at 510 K in a calculation from initial conditions corresponding to 1200 UTC on 5 Aug 1994.

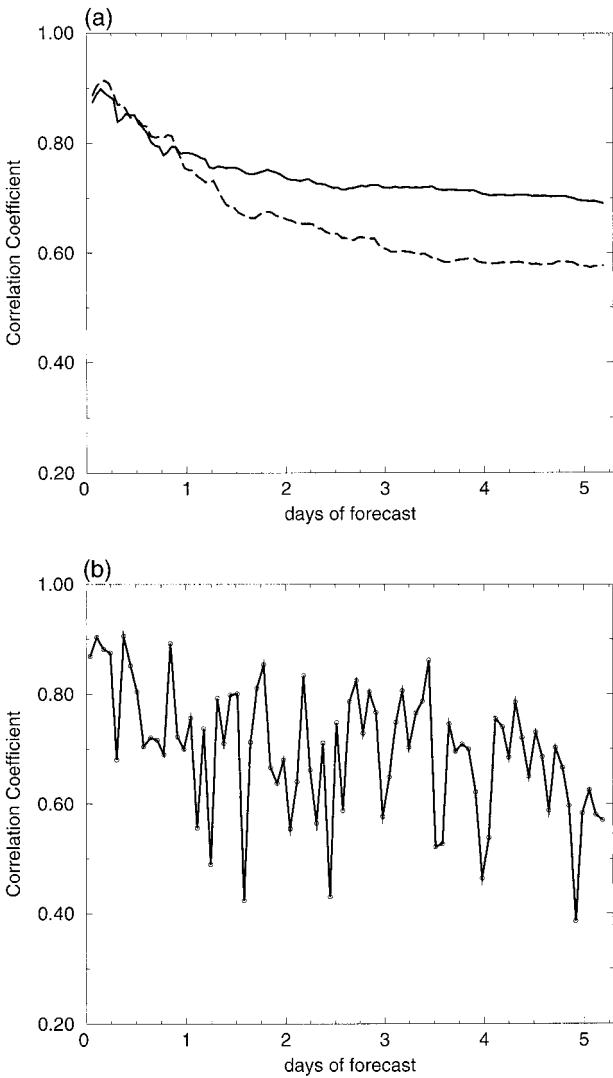


FIG. 4. Correlation (a) between MLS orbit and CAS reconstructed (area-averaged) data calculated as a function of time (solid line) and between MLS orbit and persistence of the initial ozone field (dashed line) and (b) between MLS orbit and CAS reconstructed data calculated for each *UARS* orbit (eight orbits per day).

in the band between 50° and 65°S (i.e., in the collar region), with MLS orbit mean values being larger than CAS reconstructed ones by as much as 1 ppmv. Regular fluctuations with a length scale of $\sim 5^{\circ}$ can be observed in both means, especially between 45° and 65°S . Although, as already noted, the two datasets have very different values in this region, which questions the validity of the isentropic reconstruction, the similarity in these fluctuations may be interpreted as an indication that the main features of the ozone concentration observed by MLS have counterparts among those shown in Fig. 3. Figure 5b shows that the variance of the MLS orbit data is larger than that of the CAS reconstructed data, especially in the latitude band 50° and 65°S . This is partly because MLS orbit data are not limited to the

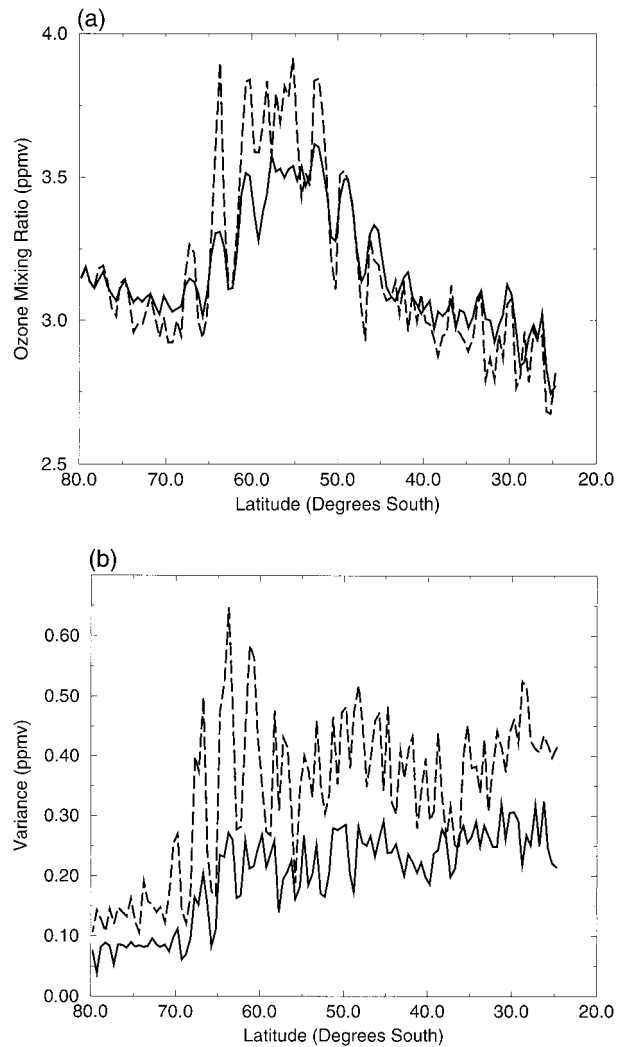


FIG. 5. MLS orbit (dashed line) and CAS reconstructed (solid line) data binned by latitude. Values are (a) means and (b) variances over the period 5–10 Aug 1994.

concentration range defined by the isolines of the CAS reconstructed data. Also, the limited accuracy of the MLS measurements (~ 0.3 ppmv) will contribute to enhance the variance associated with the MLS orbit mean.

b. Comparisons between satellite, aircraft, and CAS reconstructed ozone data

In this section we examine ozone mixing ratios from sections of flights performed by the ER-2 aircraft on 8 and 10 August 1994 at approximately 470 K (see section 2b). The data are compared with MLS synoptic data and CAS reconstructed data for the same level calculated from initial conditions on 5 August 1994. Figure 6 shows the sections along the tracks of both flights. The CAS reconstructed ozone maps at 2300 UTC on 8 and 10 August are displayed in Fig. 7, which also includes the flight path of the ER-2 aircraft.

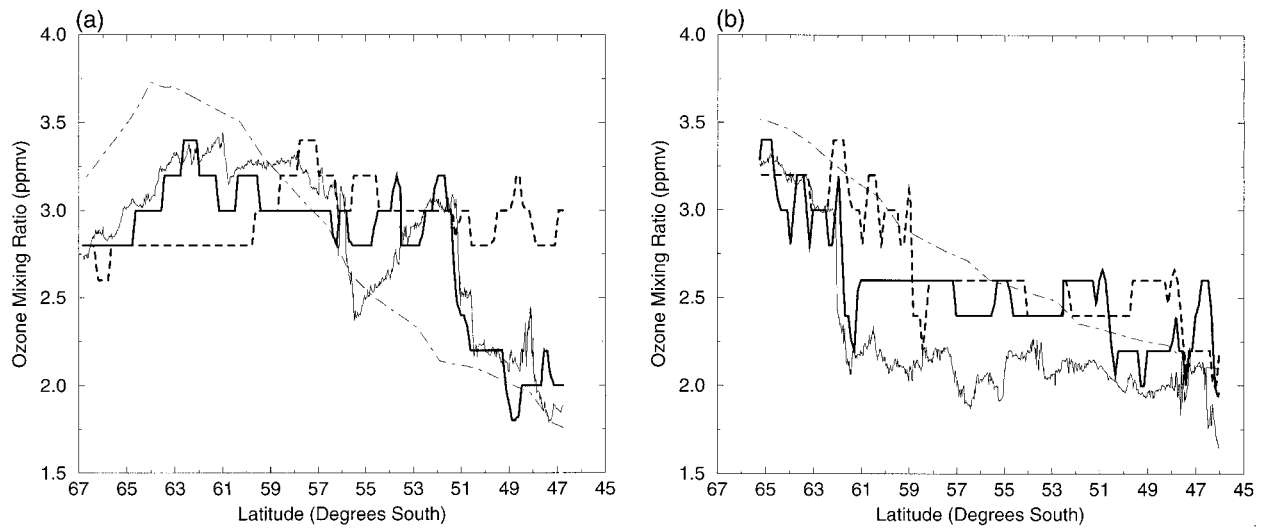


FIG. 6. Ozone mixing ratio as a function of latitude along the ER-2 aircraft flight track (a) on 8 Aug 1994 (track in Fig. 7a) and (b) on 10 Aug 1994 (track in Fig. 7b). Mixing ratios from ER-2 measurements (thin solid line) from a CAS calculation at 470 K along the ER-2 trajectory (thick dashed line) and an equatorward-shifted trajectory (thick solid) and, also at 470 K, from the MLS synoptic ozone field (dotted-dashed line).

As the ER-2 flew equatorward along the paths indicated in Figs. 7a and 7b (see Figs. 6a,b), the aircraft sampled ozone mixing ratios that decrease abruptly at latitudes 51° and 62°S, respectively. The decrease is about 1 ppmv over less than 1°. Thereon, values sampled fluctuate around a mean of about 2.25 ppmv. The corresponding MLS synoptic mixing ratios also show a decrease, but this occurs more gradually than depicted

by ER-2 data. As discussed in section 3a of this paper, ozone mixing ratio at 510 K decreases equatorward of the collar. Similarly, at 470 K, the decrease observed by the ER-2 and MLS is consistent with the transition to the outside of the collar. In addition to the local minimum at 51°S, the ER-2 dataset for 8 August (Fig. 6a) shows another local minimum with nearly the same amplitude around 56°S. The CAS reconstructed map for

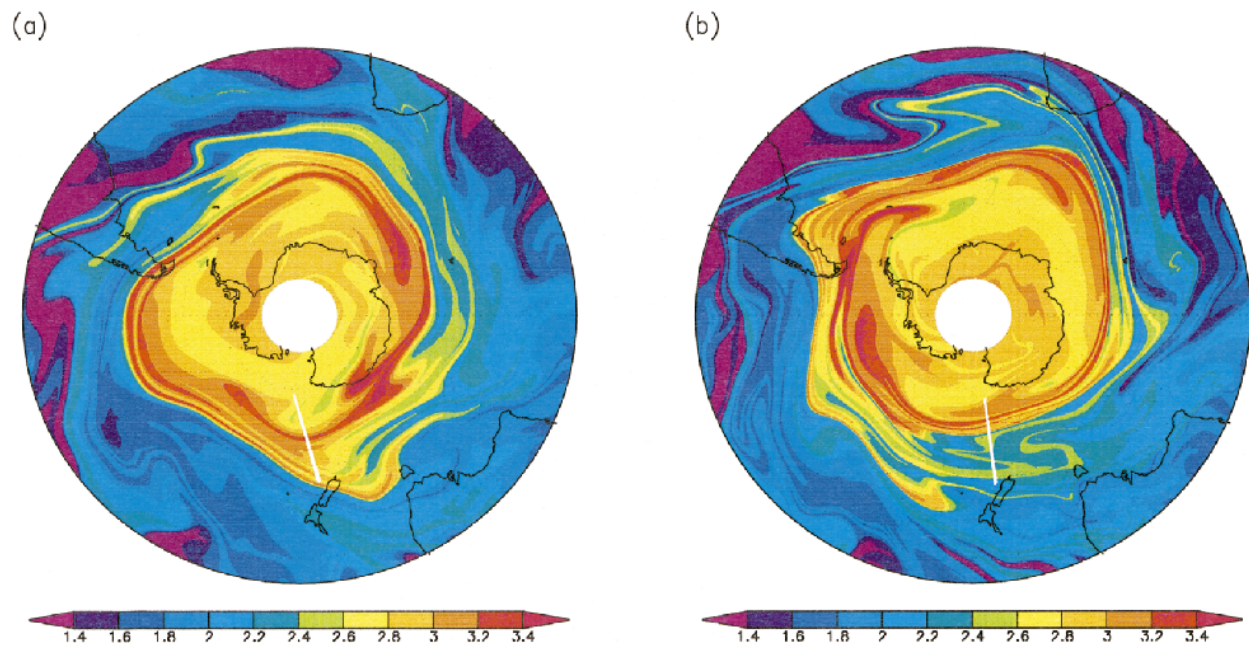


FIG. 7. CAS reconstructed map at 470 K on (a) 8 Aug 1994 at 2300 UTC, and (b) 10 Aug 1994 at 2300 UTC. The projection is stereographic about the South Pole and extends down to latitude 25°S. The track of the ER-2 flight performed around the same time is also marked on the map.

this date (Fig. 7a) shows that the flight path of the aircraft is on the outskirts of the collar on the eastward flank of a trough. At the equatorward side of the flight path there are filaments with higher mixing ratios. In Fig. 6a we report the CAS reconstructed data along the ER-2 trajectory and also along a parallel trajectory that is shifted equatorward by 5° . In this region located near a trough the CAS reconstructed data are very sensitive to phase errors in the analyzed winds and there is much improved agreement of the shifted CAS reconstructed with the observed ER-2 ozone data. Similarly, in Fig. 6b for 10 August, the MLS synoptic data do not resolve the sharp vortex boundary and the CAS reconstructed section shows a much better fit to the observations when shifted equatorward by 3° . These results suggest that CAS is able to reconstruct the small-scale features and their spatial ordering but somewhat misses the geographical location by a few degrees.

c. Diabatic descent rates in the collar region

Figure 8 shows for the same dates as Figs. 2 and 3 the descent rates at 510 K. The descent is about -1 K day^{-1} over Antarctica with a maximum over eastern Antarctica. The continent is surrounded from the central Pacific Ocean sector east to the western Indian Ocean sector by weaker descent rates of about -0.5 K day^{-1} . This descent occurs over the collar or slightly outside, and is separated from the core by a region of weak ascent. A wide and intense (up to -1.5 K day^{-1}) descent lies over the collar elsewhere, especially between Antarctica and Australia. The accuracy of these calculations is somewhat limited by the low vertical resolution of the ECMWF model in the stratosphere, but they agree fairly well with previous results (e.g., Manney et al. 1995a). Our interest here is in the geographical distribution of descent. By combining this descent with the MLS ozone profile, we have calculated the vertical ozone transport, which is shown in Fig. 9. Positive values correspond to ozone decrease, which is small but well spread inside the vortex corresponding to descent of air from depleted layers above 510 K. Negative values correspond to ozone increase, which is concentrated over the collar and is particularly strong (up to $-0.05 \text{ ppmv day}^{-1}$) south of Australia, where descent is intense. It is tempting to associate this downward transport with the ozone maximum of about $+0.1 \text{ ppmv}$ with respect to the environment that appears in this region on 9 and 10 August (see Fig. 2). There is, however, no clear correlation with such intense descent for the maxima on 6 August in the central Pacific, albeit some weak upstream precursors exist over South America and the Atlantic on 5 and 6 August. It is, therefore, plausible that the sudden ozone increases in the collar region, at least those on 9 and 10 August, are due to descent of overlying ozone-rich air.

4. Discussion and conclusions

We have analyzed the ozone evolution in the lower stratosphere of the Southern Hemisphere from 5–10 August 1994. The analysis was based on comparisons between ozone mixing ratios provided by the MLS instrument on board the *UARS*, the ER-2 UV Absorption Photometer instrument on board an ER-2 aircraft, and maps obtained with the numerical scheme of CAS. The band of maximum values in ozone mixing ratio at these altitudes, which we have referred to in this paper as the ozone collar, has been examined in relation to isentropic transport.

Outside the ozone collar, CAS reconstructed maps provide a description of how air masses may be exported from the collar outskirts to form the tongues of higher mixing ratios observed at lower latitudes on MLS synoptic fields. Despite the a priori importance of chemical effects (Anderson et al. 1989), the ozone mixing ratios outside the collar during the selected 5-day period seemed to be primarily determined by isentropic transport. In this region CAS reconstructed and MLS orbit datasets give very similar 5-day mean latitude sections. Among the various features reconstructed during the CAS calculation that show consistent relationships with MLS or ER-2 observations are filaments with transverse widths ranging from about 500 to 1000 km that can extend up to about a quarter of a hemisphere at mid-latitudes. The correlation between CAS reconstructed and MLS orbit datasets over single *UARS* orbits shows large fluctuations with comparisons giving a correlation as low as approximately 0.4 after day 1 and as high as 0.8 for some orbits around day 3. As shown by the comparison with the ER-2 data, these fluctuations may be attributed in part to discrepancies in the timing and location of corresponding features in the CAS reconstructed data and observations. These discrepancies must be compared to the uncertainties in the MLS synoptic dataset (Froidevaux et al. 1996). The quality of the wind analyses may also affect the errors. Pickering et al. (1996) compare trajectory calculations using different Southern Hemisphere wind fields and find that individual trajectories may be in error by as much as 1000 km over a 5-day-long calculation. Fairlie et al. (1997) perform a reverse domain filling calculation and noticed a poor agreement between ER-2 data and reconstructed potential vorticity values. The offset between the two datasets mentioned in this paper implies a poor score when simple correlations are computed, although a better agreement is obtained by shifting the CAS reconstruction by a few degrees.

The 5-day mean latitude sections for CAS reconstructed and MLS orbit datasets show that overall the observed location of the collar is consistent with that depicted by the CAS reconstructed maps. The CAS reconstructed CPR seems effectively isolated from the collar and, in agreement with what is observed by MLS, no CAS reconstructed filaments with collarlike mixing

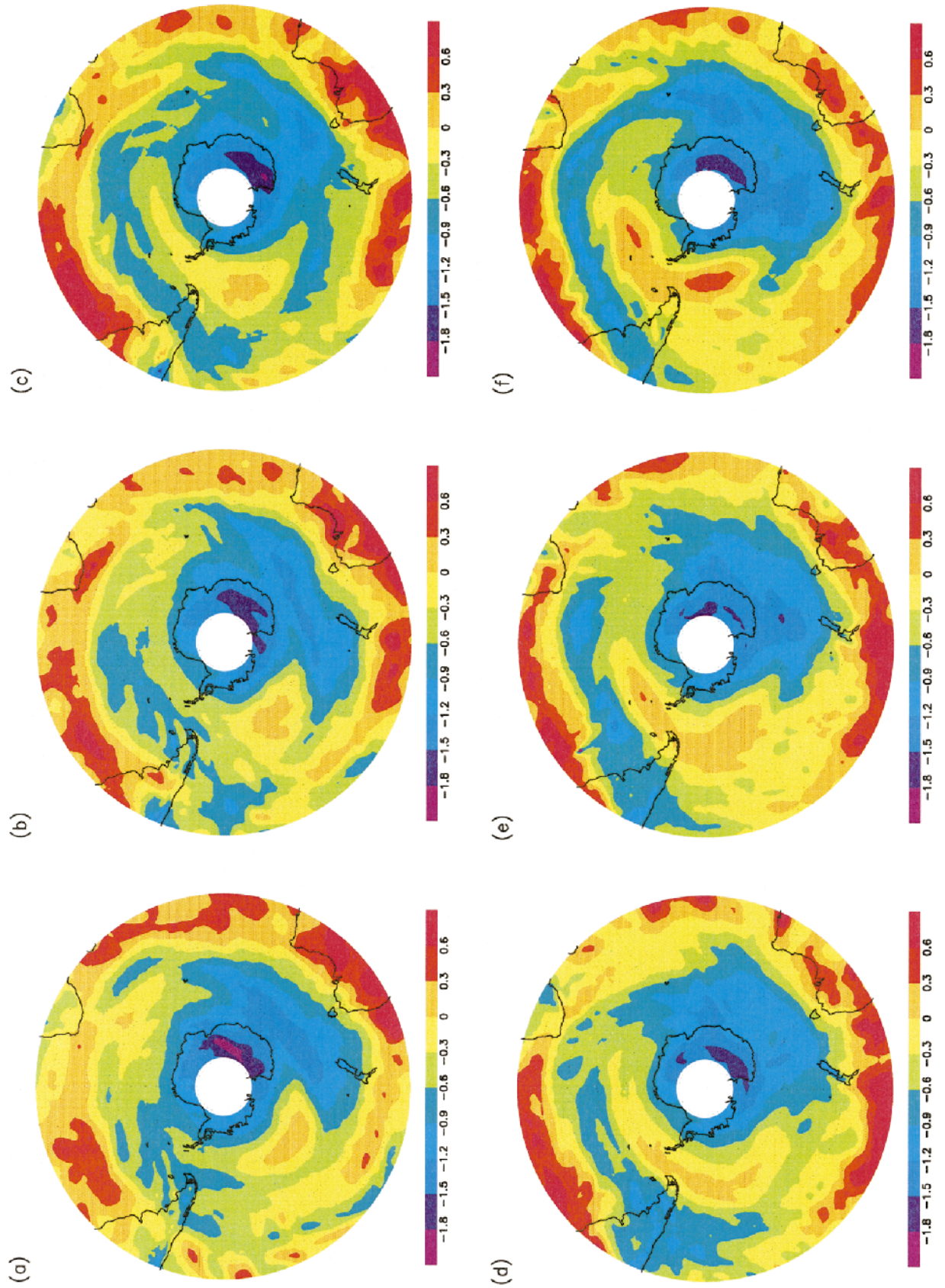


FIG. 8. Descent rate of potential temperature at 510 K and 1200 UTC on (a) 5 Aug, (b) 6 Aug, (c) 7 Aug, (d) 8 Aug, (e) 9 Aug, and (f) 10 Aug 1994. Same projection as in Fig. 2. (Scale in K day⁻¹.)

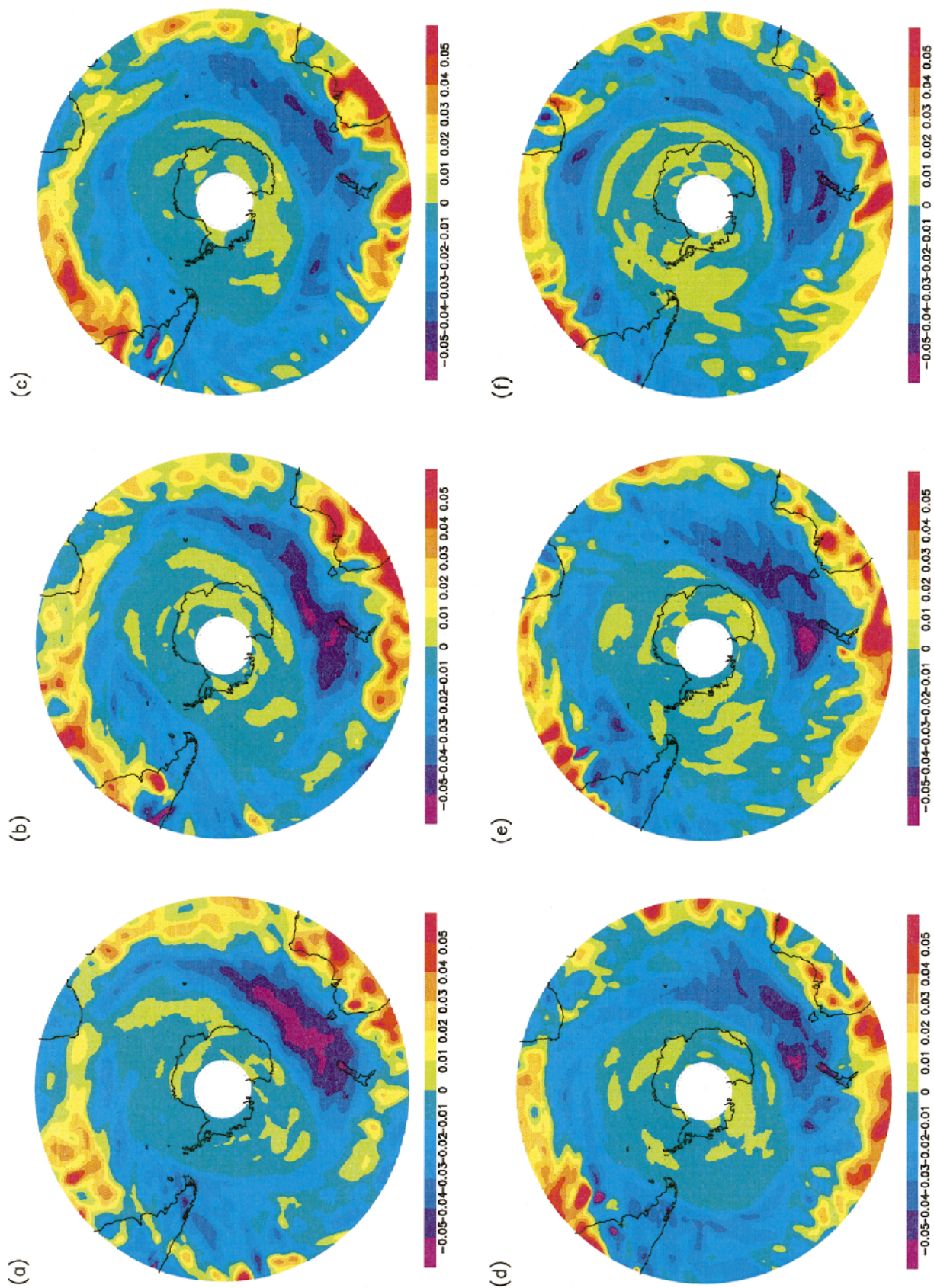


FIG. 9. As in Fig. 8, except for vertical ozone transport at 510 K as defined in the text. (Scale in ppmv day⁻¹.)

ratios are found in this region where values remain approximately constant throughout the 5-day period. Conversely, no CPR-like mixing ratios extend into the collar. This picture is consistent with the dispersion properties expected for the flow in this region (Trounday et al. 1995; Papparella et al. 1997).

The synoptic plots show that toward the end of the 5-day period, the CAS reconstructed collar tends to progressively thin out. We did not find a similar tendency in the MLS synoptic fields. The 5-day mean latitude sections between 50° and 65°S (i.e., in the collar region), show that MLS orbit mean values are larger than CAS reconstructed ones by as much as 1 ppmv and also have a larger variance. An inspection of a broader MLS dataset, for the same conditions in southern winter but for different years, suggests that an ozone collar similar to that examined here is a robust feature of the ozone distribution from mid-July to September (Waters et al. 1993; Manney et al. 1995b). A priori, the surgery component of CAS could artificially eliminate filaments from the collar when these become too thin. To gain insight into this issue, we carried out calculations changing the value of the surgery parameter δ to increase the resolution (0.0015 instead of 0.0025) but did not find substantial changes in our results. It appears, therefore, that the CAS reconstructed collar has a tendency to thin out because filaments from this region are advected to lower latitudes. This cannot be confirmed by MLS orbit data because of the limited resolution, but it seems to be supported by the ER-2 data. By calculating diabatic descent rates we show that the region of discrepancy is also that of maximum descent and ozone tendency over the collar. Therefore, we speculate that diabatic descent is responsible for maintaining the high mixing ratios observed in the ozone collar. In addition, descent can contribute to the observed shift owing to the sloping structure of the vortex. By remaining strictly isentropic, CAS misses the latitudinal shift induced by descent of the sloping structure. This hypothesis remains to be confirmed by further work.

Acknowledgments. The authors would like to acknowledge those colleagues who worked on the MLS-UARS project and the ASHOE/MAESA campaign and to thank L. Elson for providing the MLS synoptic fields. Thanks to A. Plumb, who provided helpful insights on the ASHOE/MAESA dataset, and to J. Farrara for his help with the manuscript. This research was partly supported by NASA under Grant NAGW-1021.

APPENDIX

The CAS Algorithm

The initial condition for the CAS algorithm (Vaugh and Plumb 1994; Norton 1994) is a set of N isolines corresponding to selected values of the tracer's concentration. Nodes are distributed along the isolines to define

the initial contours. The evolution of the tracer is reconstructed by advecting the contour nodes with observed winds; accuracy is maintained by periodically redistributing the nodes and applying contour surgery (Dritschel 1989). The redistribution of the nodes along the contours is operated according to the local curvature with a density depending on a parameter μ . The surgery splits one contour into two or merges together two contours defining the same isoline when segments get closer than a critical distance defined by the parameter δ .

The validity of this approach for investigation of stratospheric motions has been established by Vaugh et al. (1994). Our calculations use the CAS implementation presented in Mariotti et al. (1997) and use parameter values $m = 0.1$ and $\delta = 0.0025$, following Vaugh et al. (1994).

REFERENCES

- Anderson, J. G., W. H. Brune, and M. H. Proffitt, 1989: Ozone destruction by chlorine radicals within the antarctic vortex: The spatial and temporal evolution of ClO-O₃ anticorrelation based on in situ ER-2 data. *J. Geophys. Res.*, **94** (D9), 11 465–11 479.
- Barath, F. T., and Coauthors, 1993: The Upper Atmosphere Research Satellite Microwave Limb Sounder instrument. *J. Geophys. Res.*, **98** (D6), 10 751–10 762.
- Bowman, K. P., 1993: Large scale isentropic mixing properties of the Antarctic polar vortex from analyzed winds. *J. Geophys. Res.*, **98** (D12), 23 013–23 027.
- , and N. J. Mangus, 1993: Observations of deformation and mixing of the total ozone field in the Antarctic polar vortex. *J. Atmos. Sci.*, **50**, 2915–2921.
- Brunet, G., R. Vautard, B. Legras, and S. Edouards, 1995: Potential vorticity on isentropic surfaces: Climatology and diagnostics. *Mon. Wea. Rev.*, **123**, 1037–1058.
- Chen, P., 1994: The permeability of the Antarctic vortex edge. *J. Geophys. Res.*, **99** (D10), 20 563–20 5721.
- , J. R. Holton, A. O'Neill, and R. Swinbank, 1994: Quasi-horizontal transport and mixing in the Antarctic stratosphere. *J. Geophys. Res.*, **99** (D8), 16 851–16 866.
- Chipperfield, M. P., E. R. Lutman, J. A. Kettleborough, J. A. Pyle, and A. E. Roche, 1997: Model studies of chlorine deactivation and formation of ClONO₂ collar in the Arctic polar vortex. *J. Geophys. Res.*, **102** (D1), 1467–1478.
- Dritschel, D., 1989: Contour dynamics and contour surgery: Numerical algorithms for extended, high-resolution modelling of vortex dynamics in two-dimensional, inviscid, incompressible flows. *Comput. Phys. Rep.*, **10**, 77–146.
- Elson, L., and L. Froidevaux, 1993: Use of Fourier transforms for asymptotic mapping: Applications to the Upper Atmosphere Research Satellite Microwave Limb Sounder. *J. Geophys. Res.*, **98** (D12), 23 039–23 049.
- Fairlie, T. D., R. B. Pierce, W. L. Grose, G. Lingenfelter, M. Loewenstein, and J. R. Podolske, 1997: Lagrangian forecasting during ASHOE/MAESA: Analysis of predictive skill for analyzed and reverse-domain-filled potential vorticity. *J. Geophys. Res.*, **102**, 13 169–13 182.
- Froidevaux, L., and Coauthors, 1996: Validation of UARS Microwave Limb Sounder ozone measurements. *J. Geophys. Res.*, **101** (D6), 10 017–10 060.
- Hartmann, D. L., and Coauthors, 1989: Potential vorticity and mixing in the south polar vortex during spring. *J. Geophys. Res.*, **94**, 11 625–11 640.
- Juckes, M. N., and M. E. McIntyre, 1987: A high resolution one layer model of breaking planetary waves in the stratosphere. *Nature*, **328**, 590–596.

- Manney, G. L., and Coauthors, 1995a: Lagrangian transport calculations using *UARS* data. Part I: Passive tracers. *J. Atmos. Sci.*, **52**, 3049–3068.
- , L. Froidevaux, J. W. Waters, and R. W. Zurek, 1995b: Evolution of microwave limb sounder ozone and the polar vortex during winter. *J. Geophys. Res.*, **100** (D2), 2953–2972.
- , R. W. Zurek, L. Froidevaux, J. W. Waters, A. O'Neill, and R. Swinbank, 1995c: Lagrangian transport calculations using *UARS* data. Part II: Ozone. *J. Atmos. Sci.*, **52**, 3069–3081.
- Mariotti, A., M. Moustauoui, B. Legras, and H. Teitelbaum, 1997: Comparison between vertical ozone soundings and reconstructed potential vorticity maps by contour advection with surgery. *J. Geophys. Res.*, **102** (D5), 6131–6142.
- McIntyre, M. E., 1989: On the Antarctic ozone hole. *J. Atmos. Terr. Phys.*, **51**, 29–43.
- Morcrette, J. J., 1991: Radiation and cloud radiative properties in the European Centre for Medium Range Weather Forecasts forecasting system. *J. Geophys. Res.*, **96** (D5), 9121–9132.
- Morris, G. A., and Coauthors, 1995: Trajectory mapping and applications to data from the Upper Atmosphere Research satellite. *J. Geophys. Res.*, **100** (D8), 16 491–16 505.
- Newman, P. A., and Coauthors, 1996: Measurements of polar vortex air in the midlatitudes. *J. Geophys. Res.*, **101** (D8), 12 879–12 891.
- Norton, W. A., 1994: Breaking Rossby waves in a model stratosphere diagnosed by a vortex-following coordinate system and a technique for advecting material contours. *J. Atmos. Sci.*, **51**, 654–673.
- Orsolini, Y. J., G. Hansen, U.-P. Hoppe, G. L. Manney, and K. H. Fricke, 1997: Dynamical modelling of wintertime lidar observations in the Arctic: Ozone laminae and ozone depletion. *Quart. J. Roy. Meteor. Soc.*, **123**, 785–800.
- Pierce, R. B., T. D. Fairlie, W. L. Grose, R. Swinbank, and A. O'Neill, 1994: Mixing processes within the polar night jet. *J. Atmos. Sci.*, **51**, 2957–2972.
- Papparella, F., A. Babiano, C. Basdevant, A. Provenzale, and P. Tanga, 1997: A Lagrangian study of the Antarctic polar vortex. *J. Geophys. Res.*, **102** (D6), 6765–6773.
- Pickering, K. E., and Coauthors, 1996: TRACE a trajectory inter-comparison. Part I: Effects of different input analyses. *J. Geophys. Res.*, **101** (D19), 23 909–23 925.
- Polvani, L. and R. Plumb, 1992: Rossby wave breaking, micro-breaking, filamentation, and secondary vortex formation: The dynamics of a perturbed vortex. *J. Atmos. Sci.*, **49**, 462–476.
- Proffitt, M. H., and Coauthors, 1989: In situ ozone measurements within the 1987 ozone hole from a high-latitude ER-2 aircraft. *J. Geophys. Res.*, **94**, 16 547–16 556.
- Reber, C., 1990: The Upper Stratosphere Research Satellite. *Eos, Trans. Amer. Geophys. Union*, **71**, 1867–1878.
- Roche, A. E., and Coauthors, 1994: Observations of lower-stratospheric ClONO₂, HNO₃ and aerosol by the UARS CLAES experiment between January 1992 and April 1993. *J. Atmos. Sci.*, **51**, 2877–2902.
- Rosenfield, J. E., P. A. Newman, and M. R. Schoeberl, 1994: Computation of the diabatic descent in the stratospheric polar vortex. *J. Geophys. Res.*, **99** (D8), 16 677–16 689.
- Schoeberl, M. R., and D. L. Hartmann, 1991: The dynamics of the stratospheric polar vortex and its relation to springtime ozone depletion. *Science*, **251**, 46–52.
- , and P. A. Newman, 1995: A multiple-level trajectory analysis of vortex filaments. *J. Geophys. Res.*, **100** (D12), 25 801–25 815.
- , L. R. Lait, P. A. Newman, and J. E. Rosenfield, 1992: The structure of the polar vortex. *J. Geophys. Res.*, **97** (D8), 7859–7882.
- Sutton, R., H. MacLean, R. Swinbank, A. O'Neill, and F. W. Taylor, 1994: High-resolution stratospheric tracer fields estimated from satellite observations using lagrangian trajectory calculations. *J. Atmos. Sci.*, **51**, 2995–3005.
- Trunday, B. L., L. Perthuis, S. Strebelle, J. D. Farrara, and C. R. Mechoso, 1995: Dispersion properties of the flow in the southern stratosphere during winter and spring. *J. Geophys. Res.*, **100**, 13 901–13 917.
- Tuck, A. T., W. H. Brune, and R. S. Hipskind, 1997: Airborne Southern Hemisphere Ozone Experiment/Measurements for Assessing the Effects of Stratospheric Aircrafts (ASHOE/MAESA): A road map. *J. Geophys. Res.*, **102** (D3), 3901–3904.
- Waters, J. W., 1993: Microwave limb sounding. *Atmospheric Remote Sensing by Microwave Radiometry*, M. Janssen, Ed., Wiley, 383–496.
- , L. Froidevaux, G. L. Manney, W. G. Read, and L. S. Elson, 1993: MLS observations of lower stratospheric ClO and O₃ in the 1992 Southern Hemisphere winter. *Geophys. Res. Lett.*, **20**, 1219–1222.
- Waugh, D., and R. Plumb, 1994: Contour advection with surgery: A technique for investigating fine scale structure in tracer transport. *J. Atmos. Sci.*, **51**, 530–540.
- , and Coauthors, 1994: Transport of material out of the stratospheric Arctic vortex by Rossby wave breaking. *J. Geophys. Res.*, **99** (D1), 1071–1088.